biosensors

MDPI

Article

Surface Modification of Screen-Printed Carbon Electrode through Oxygen Plasma to Enhance Biosensor Sensitivity

Shuto Osaki [1,*], Masato Saito [1,2], Hidenori Nagai [1] and Eiichi Tamiya [1,3,*]

[1] AIST-Osaka University Advanced Photonics and Biosensing Open Innovation Laboratory, National Institute of Advanced Industrial Science and Technology, Photonics Center, Osaka University, 2-1 Yamadaoka, Suita 565-0871, Osaka, Japan; hide.nagai@aist.go.jp (H.N.)
[2] Graduate School of Engineering, Osaka University, 2-1 Yamadaoka, Suita 565-0871, Osaka, Japan
[3] SANKEN-The Institute of Scientific and Industrial Research, Osaka University, 8-1 Mihogaoka, Ibaraki 567-0047, Osaka, Japan
* Correspondence: shuto-osaki@aist.go.jp (S.O.); tamiya@ap.eng.osaka-u.ac.jp (E.T.)

Abstract: The screen-printed carbon electrode (SPCE) is a useful technology that has been widely used in the practical application of biosensors oriented to point-of-care testing (POCT) due to its characteristics of cost-effectiveness, disposability, miniaturization, wide potential window, and simple electrode design. Compared with gold or platinum electrodes, surface modification is difficult because the carbon surface is chemically or physically stable. Oxygen plasma (O_2) can easily produce carboxyl groups on the carbon surface, which act as scaffolds for covalent bonds. However, the effect of O_2-plasma treatment on electrode performance remains to be investigated from an electrochemical perspective, and sensor performance can be improved by clarifying the surface conditions of plasma-treated biosensors. In this research, we compared antibody modification by plasma treatment and physical adsorption, using our novel immunosensor based on gold nanoparticles (AuNPs). Consequently, the O_2-plasma treatment produced carboxyl groups on the electrode surface that changed the electrochemical properties owing to electrostatic interactions. In this study, we compared the following four cases of SPCE modification: O_2-plasma-treated electrode/covalent-bonded antibody (a); O_2-plasma-treated electrode/physical adsorbed antibody (b); bare electrode/covalent-bonded antibody (c); and bare electrode/physical absorbed antibody (d). The limits of detection (LOD) were 0.50 ng/mL (a), 9.7 ng/mL (b), 0.54 ng/mL (c), and 1.2 ng/mL (d). The slopes of the linear response range were 0.039, 0.029, 0.014, and 0.022. The LOD of (a) was 2.4 times higher than the conventional condition (d), The slope of (a) showed higher sensitivity than other cases (b~d). This is because the plasma treatment generated many carboxyl groups and increased the number of antibody adsorption sites. In summary, the O_2-plasma treatment was found to modify the electrode surface conditions and improve the amount of antibody modifications. In the future, O_2-plasma treatment could be used as a simple method for modifying various molecular recognition elements on printed carbon electrodes.

Keywords: electrochemical immunosensor; gold nanoparticles; oxygen plasma; point-of-care; biosensors

Citation: Osaki, S.; Saito, M.; Nagai, H.; Tamiya, E. Surface Modification of Screen-Printed Carbon Electrode through Oxygen Plasma to Enhance Biosensor Sensitivity. *Biosensors* **2024**, *14*, 165. https://doi.org/10.3390/bios14040165

Received: 29 January 2024
Revised: 25 March 2024
Accepted: 25 March 2024
Published: 29 March 2024

1. Introduction

The screen-printed carbon electrode (SPCE) is a useful technology that has been widely used in the practical application of biosensors oriented toward point-of-care testing (POCT) [1–7]. Many researchers have reported on electrochemical biosensors that use SPCE to detect hormones [8–10], ions [11,12], metals [13], nucleic acid [14–19], and proteins [20–23]. Although the sensitivity of the electrochemical biosensor is controlled by surface conditions, such as the diffusion coefficient and electron transfer rate [24], these are altered by the modification of molecular recognition elements and blocking materials on the electrode surface. We previously reported on biosensors that use redox reactions of gold nanoparticles and found that antibodies and blocking materials modified on the electrode reduced the diffusion coefficient and electron transfer rate [25]. As it is necessary to measure very small

amounts of biomarkers to achieve POCT, electrochemical biosensors with higher sensitivity and selectivity are required. Therefore, a more efficient method for modifying molecular recognition elements, such as antibodies, without degrading their electrochemical properties is required. However, compared to gold or platinum electrodes, the surface modification of SPCEs is difficult because the carbon surface is chemically or physically stable [26]. For gold or platinum electrodes, a self-assembled monolayer (SAM) based on alkanethiol is mainly used for antibody modification [27–32]. Aptamers modified with a thiol group are also used, based on the same principle [33]. In addition, drop-casted biopolymers and nanomaterials do not depend on the electrode material [16,34–41].

For the carbon electrode, the direct production of a carboxyl group, which acts as a scaffold for the covalent bonds on the carbon surface using electrochemical activation, has been reported [42–44]. For example, the SPCE surface was activated to produce a carboxyl group by applying a potential of 0.9 V for 60 s in a 0.5 M acetate buffer (ABS, pH 4.80) [45] or 1.0 V for 50 s in a 0.10 M sulfuric acid solution [46]. Oxygen plasma (O_2-plasma) treatment is an efficient technique for producing carboxyl groups on the surface [47–49] and is used for surface cleaning and regeneration [50,51].

However, regarding SPCE, there have been no reports of antibody modification by generating carboxyl groups using O_2-plasma treatment, and only improvements in electrochemical performance have been discussed. For example, O_2 plasma is used to remove the binder from carbon inks and control the surface roughness of SPCE [52–57].

In this study, we compared antibody modification by O_2-plasma treatment and physical adsorption using our novel immunosensor, which is a gold-linked electrochemical immunoassay (GLEIA). This biosensor is based on a sandwich-type immunoassay applied directly on the electrode and detects the antigen concentration through the redox current of gold nanoparticles (AuNPs) modified with a secondary antibody [5,25,58–62]. Specifically, the AuNPs on the electrode are oxidized at a high potential to produce gold ions, and the concentration of nanoparticles is quantified by measuring the reduction current of gold ions. The chemical reaction is $Au + Cl_4 \rightleftarrows AuCl_4 + 3e$ (E_0 = 0.803 V, vs. Ag/AgCl sat.). We previously reported that physically adsorbed antibodies decrease the electrochemical reaction rate because they act as a resistance on the electrode [25]. Thus, O_2-plasma and covalent bonding reagents can be used as an alternative antibody-modification method to physical adsorption. We investigated the O_2-plasma-treated surface by cyclic voltammetry (CV), scanning electron microscopy (SEM), X-ray photoelectron spectroscopy (XPS), and contact angle analysis. Consequently, the generation of carboxyl groups on the electrode surface, changes in the surface charge, increased capacitance, and hydrophilicity were observed. These changes can be explained by the generation of carboxyl groups on the electrode surface, indicating that O_2-plasma treatment is a simple and effective surface modification method. We also observed that the O_2-plasma-treated electrode showed higher sensitivity than the electrode without O_2-plasma for immunoglobulin A (IgA) because the covalently bonded antibody inhibited nonspecific adsorption with the abovementioned changes on the surface.

2. Materials and Methods

2.1. Reagents

All reagents used were of guaranteed grade and used without further purification. All inorganic salts, 1-Ethyl-3-(3dimethylaminopropyl) carbodiimide ·HCl (EDC), N-hydroxysuccinimide (NHS), polyethylene glycol (Mw is 20,000), trehalose dihydrate, and pH 7.5 D-PBS (-) were purchased from Fujifilm Wako Pure Chemicals (Osaka, Japan). AuNPs with diameters of 60 nm were purchased from BBI Solutions (Cardiff, UK). Anti-IgA (α), Human, Goat-Poly, A80-102A, and Purified Human IgA, P80-102 were purchased from Bethyl Laboratory (Montgomery, AL, USA). Bovine serum albumin (BSA) was purchased from Jackson Immunoresearch (West Grove, PA, USA). All water used in this study was Milli-Q water (18.3 MΩ cm).

2.2. Instruments

A miniSTAT400 potentiostat was purchased from BioDevice Technology (Ishikawa, Japan). A disposable screen-printed carbon electrode (DEP-EP-PP) with an integrated working electrode (surface area: 2.64 mm^2), counter electrode, and Ag/AgCl reference electrode, with a total length of 11 mm, was also purchased from BioDevice Technology. All electrochemical measurements were performed by dropping 20 µL of the sample onto the printed electrode, unless otherwise stated. A UV-visible spectrometer (DS-11+) was purchased from Denovix (Wilmington, DE, USA). A micro-high-speed cooling centrifuge (kitman-24) was purchased from Tomy Seiko (Tokyo, Japan). An O_2-plasma cleaner (PDC210) was purchased from Yamato Scientific (Tokyo, Japan). Scanning electron microscopy (SEM) was performed using an S-4800 (Hitachi High-Tech, Tokyo, Japan). X-ray photoelectron spectroscopy (XPS) analysis was performed by Toray Research Center (Tokyo, Japan) using a Quantera SXM (Ulvac-PHI). Contact angle analysis was performed using a DMo-602 instrument obtained from Kyowa Interface Science (Saitama, Japan). Electrochemical Impedance Spectroscopy was performed by Autolab PGSTAT 14N (Metrohm Autolab Utrecht, Kanaalweg 29G, Utrecht, The Netherlands).

2.3. Electrochemical Analysis of O_2-Plasma-Treated Electrodes

The O_2-plasma treatment was performed in a 13.56 MHz ratio frequency (RF) plasma reactor. The SPCE, with a cyclo-olefin polymer (COP) film covering the connector part and reference electrode, was placed in the reactor. After the reactor was first evacuated to a base pressure of less than 10^{-3} Pa, 200 cc O_2 gas was introduced. The O_2-plasma treatment of the SPCE was performed at 75 W plasma power for a period of 5 s. The electrode was evaluated using cyclic voltammetry (CV) with the standard electrochemical mediators: potassium ferricyanide and hexaammineruthenium(III) chloride, each containing 100 mM of Na_2SO_4 as the electrolyte,. For the ferricyanide, the sweep rates were 10 to 250 mV/s, and the sweep range was −400 to 600 mV. For the ruthenium, the sweep rates were 10 to 200 mV/s, and the sweep range was 700 to −700 mV. Electrochemical impedance spectroscopy (EIS) was also used to evaluate the kinetic parameters within the frequency range of 100 kHz to 0.1 Hz applied potential, superimposed on a DC potential of 0.1 V, with an AC of 10 mV peak-to-peak amplitude under 5 mM ferricyanide and 100 mM Na_2SO_4.

2.4. Surface Analysis of O_2-Plasma-Treated Electrodes

The electrode surface was analyzed by SEM, XPS, and contact angle measurement. SEM was used to observe the electrode surface after the antigen-antibody reaction to evaluate the AuNPs present on the surface. For this purpose, X-rays (monochromatic Al K∝ ray) of 200 µm diameter were irradiated on the electrodes, which were stored in light-shielded vacuum gauges prior to the XPS analysis. The contact angle measurement was conducted using water drops (2 µL). The drops were placed on the working electrode, the needle was pulsed back, and the drop shape was immediately captured using the camera. The obtained images from the electrodes were analyzed using FAMAS software (ver. 7.2.0 from Kyowa Interface Science Co., Ltd.) to determine the circle fitting.

2.5. Antibody Modification

The electrode surface was modified via physical adsorption and covalent bonding to compare the response of the sensor to the antibody modification process. For the physical adsorption, 2 µL of 50 µg/mL antibody in PBS was dropped onto the working electrode and incubated at 4 °C for 1 h to adsorb the antibody. Next, 20 µL of 1% BSA in PBS solution was dropped onto the entire electrode and incubated at room temperature (RM) for 1 h. For covalent bonding, 50:50 mM of EDC/NHS solution was dropped onto the working electrode and incubated for 30 min. Next, 2 µL of 50 ug/mL antibody in PBS was placed on the electrodes and incubated for 30 min. Finally, 20 µL of 1% BSA in PBS solution was dropped onto the entire electrode and incubated at RM for 30 min (see Scheme 1). The prepared electrode was stored at 4 °C until use.

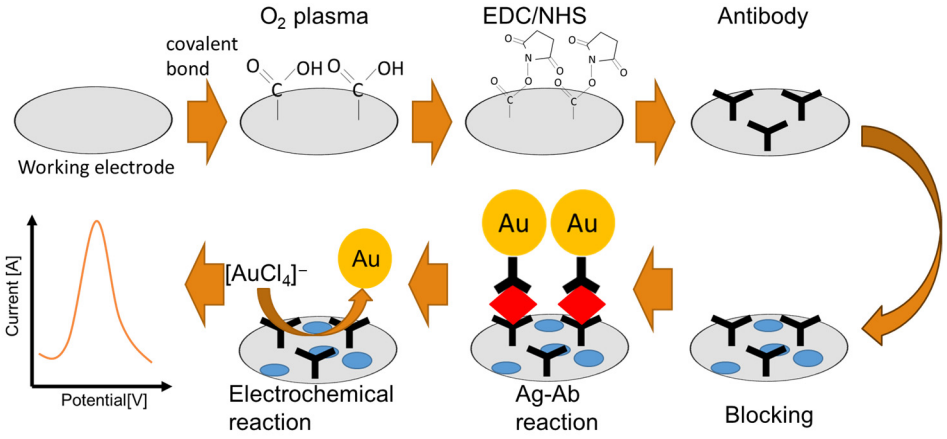

Scheme 1. Schematic illustration of the biosensor fabrication and sensing flow.

2.6. Preparing Secondary Antibody-Modified Gold Nanoparticles

Secondary antibody-modified AuNPs were prepared using a reported method [5]. Then, the 0.9 mL of AuNP solution was mixed with the 0.1 mL of phosphate buffer (Na_2HPO_4/NaH_2PO_4, 50 mM, pH 7.5). 50 µg/mL of Anti-IgA was added to the Au nanoparticle solution to dissolve the 5 mM of phosphate buffer (pH 7.5) and kept for 10 min at RM. Hereinafter, this is referred to as the Au conjugate. Then, 0.1 mL of 10% BSA in PBS buffer and 0.05 mL of 1% PEG in PBS buffer were added to the Au conjugate. The Au Anti-IgA conjugate was collected by centrifugal operation (4000× *g* for 20 min at 4 °C). After centrifugation, the Au Anti-IgA conjugate was suspended in 1 mL of preservation solution (1% BSA, 0.05% PEG 20000, 0.1% NaN_3, and 150 mM NaCl in 20 mM Tris-HCl buffer, pH 8.2) and collected again in the same manner. For the stock solution, the Au Anti-IgA conjugate was suspended in the preservation solution, and the optical density was adjusted to OD_{520} = 6. The Au Anti-IgA conjugate was diluted 3 times with 50 *w/v* of trehalose (OD_{520} = 2) and by dripping 5 µL of this solution in the 96 wells. Then, the 96-well plate was dried in a vacuum condition for 5 min. Dried wells were stored at 4 °C until use.

2.7. Immunosensor Fabrication Using O_2-Plasma-Treated SPCE

A sandwich type antigen–antibody (Ab–Ag) reaction occurred directly on the working electrode (Scheme 1). IgA antigen solutions (100–0 ng/mL) were prepared by dilution in PBS. A total of 10 µL of the IgA solution was dropped in the prepared 96-well plate and mixed for 10 s. After 1 min, 2.0 µL of the solution was placed on the working electrode to incubate for 1 h at RM in the closed box with damped cotton (to maintain humidity to prevent the sample from drying). After rinsing with PBS and eliminating the PBS solution with N_2 air, the direct redox reaction was performed in 2 M KCl solution (20 µL) covering the entire electrode at RM. The pre-oxidation and differential pulse voltammetry (DPV) parameters were as follows: the beginning and end potentials were 800 and 200 mV, the step potential was 4 mV, pulse amplitude (pulse potential) was 100 mV, pulse period was 200 ms, pulse width was 50 ms, and sampling width was set to 16 ms. All conditions were optimized in our previous work [25].

3. Results and Discussion

3.1. Comparing the Surface Change by Electrochemical Kinetics Parameters

Figure 1a–d shows the cyclic voltammograms of 5 mM ferricyanide and ruthenium complex on the bare and O_2-plasma-treated electrodes. Among these voltammograms, the electrochemical reaction is a reversible process because of the peak separations at the 50 mV/s scan rate of 152, 190, 286, and 178 mV. Figure 2a,b shows the relationship between

the peak current intensity and the square root of the scan rate. The diffusion coefficient for the reversible process was calculated using the following equation:

$$I_{p,cv} = -\left(2.69 \times 10^5\right) n^{\frac{3}{2}} A C_{bulk} D^{\frac{1}{2}} v^{\frac{1}{2}} \quad (1)$$

where n is the number of electrons in the reaction, A is the electrode area, C_{bulk} is the concentration of the electrochemical mediators, and v is the scan rate.

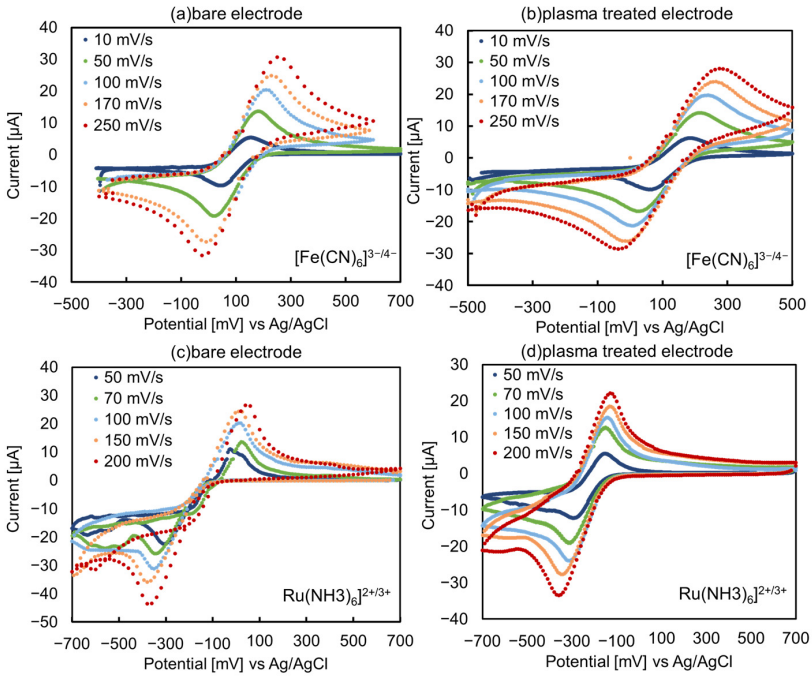

Figure 1. Cyclic voltammograms of 5 mM ferricyanide and 5 mM ruthenium complex on the bare (**a**,**c**); and plasma-treated electrodes (**b**,**d**).

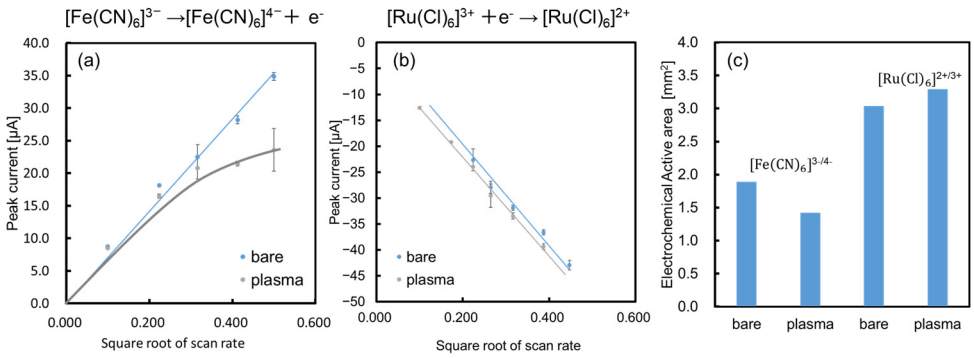

Figure 2. Relationship between peak current intensity and square root of scan rate for ferricyanide (**a**); and ruthenium complex (**b**). Electrochemical active areas of ferricyanide and ruthenium complex on bare electrode and O_2-plasma-treated electrode (**c**).

The electroactive area of the two types of electrochemical mediators (ferricyanide and ruthenium complex) at both electrodes (bare and plasma) were calculated using Equation (1) and the diffusion coefficients were determined with results from a previous study. Both of the diffusion coefficients are 7.75×10^{-6} cm^2/s for ferricyanide, and 5.77×10^{-6} cm^2/s for ruthenium complex obtained from [63]. The effective electroactive areas ($A_{bare,\ Fe}$, $A_{plasma,\ Fe}$ and $A_{bare,Ru}$ and $A_{plasma,\ Ru}$) were 1.89 mm^2, 1.42 mm^2, 3.04 mm^2 and 3.29 mm^2, as summarized in Figure 2c.

From the results, it was observed that the electroactivity of the negatively charged ferricyanides decreased and that the positively charged ruthenium complexes slightly increased at the O_2-plasma-treated electrode. Electrostatic repulsion for the ferricyanide may occur due to the negative charge of the carboxyl groups generated by the plasma treatment. For the positively charged ruthenium complex, instead of electrostatic repulsion not occurring, diffusion to the electrodes could have been promoted. Electrostatic repulsion occurs between dendrimers and electrochemical mediators on the electrode surface [64], indicating a close relationship between the surface charge and electrochemical activity.

Next, charge transfer resistance (*Rct*) and capacitance (*Cdl*) were evaluated using EIS. Figure 3a shows the Cole-Cole plots of both electrodes in 5 mM of ferricyanide. The bare electrode showed a clear semicircle, while the O_2-plasma-treated electrode showed partial disappearance of the semicircle. Based on these results, *Cdl* and *Rct* were obtained by fitting using the equivalent circuit. The plasma treatment did not change *Rct*, but increased *Cdl* (Figure 3b,c). This result supports the aforementioned surface charge change.

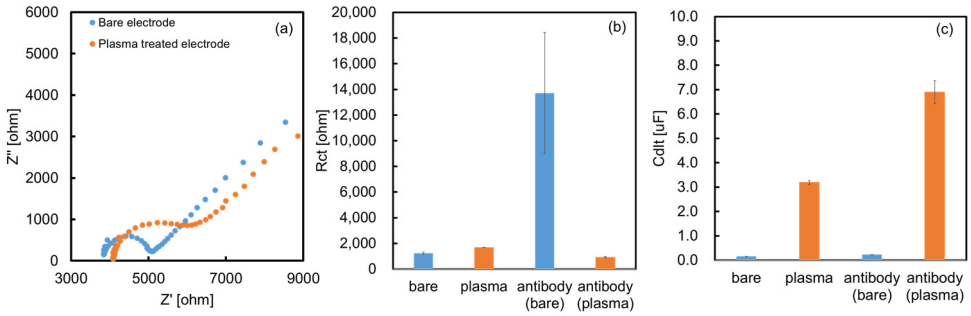

Figure 3. Cole-Cole plot of bare electrode and plasma-treated electrode in the 5 mM of ferricyanide (**a**); *Rct* value (**b**); and *Cdl* (**c**).

Therefore, the O_2-plasma treatment changes the surface charge of the electrode and alters its electrochemical properties. Surface analysis using XPS suggested that this change in surface charge was due to the formation of carboxyl groups (Figure 4). Our results did not show any improvement in the electrode performance owing to the removal of impurities or binders in the SPCE. On the contrary, electrostatic interactions with reactive species and an improvement in hydrophilicity were observed due to the generation of the carboxyl groups. These results depend on the electrode materials and plasma irradiation conditions, indicating that individual optimization is required.

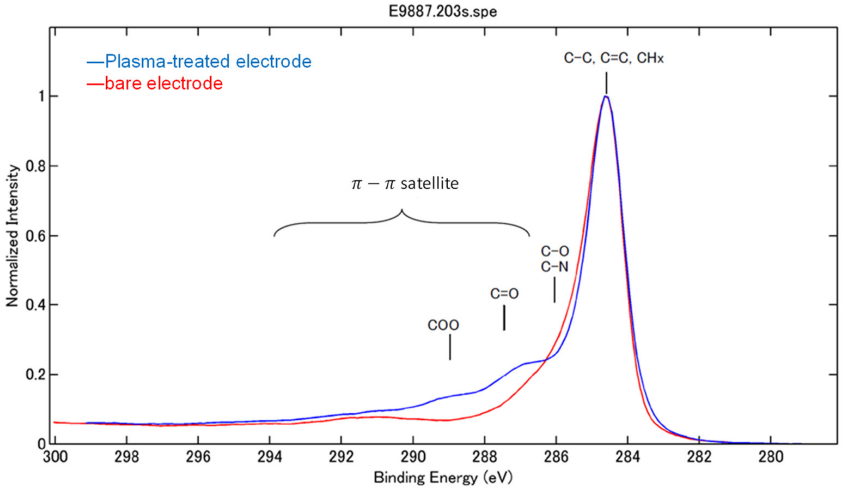

Figure 4. XPS spectra of plasma-treated electrode (blue line) and bare electrode (red line).

We also performed EIS measurements on the electrode after antibody modification. The results are shown in Figure 3b,c, where *Rct* increased when the antibody was modified by physical adsorption, and *Cdl* increased when it was modified by covalent bonding. These contrasting results are interesting and may indicate differences in the orientation and adsorption conditions of the antibody on each electrode. The antibody simply functions as an insulator because it is physically adsorbed on the bare electrodes and increases *Rct*. However, a gap occurs between the antibody and electrode because the antibody is modified by covalent bonding at the O_2-plasma-treated electrode. Consequently, electrode resistance did not occur; instead, the electric double layer capacitance was altered by the electric charge of the antibody.

3.2. Sensor Characteristics

Figure 5 shows differential pulse voltammograms of the biosensor using O_2-plasma-treated/covalent bonding (a), O_2-plasma-treated electrode/physical adsorption (b), bare electrode/covalent bonding (c), and bare electrode/physical adsorption (d). Blank signals (0 ng/mL of IgA) were suppressed when covalent bonding was used (Figure 5a,c). The peak currents to 100 ng/mL of IgA were almost constant, except in Figure 5c.

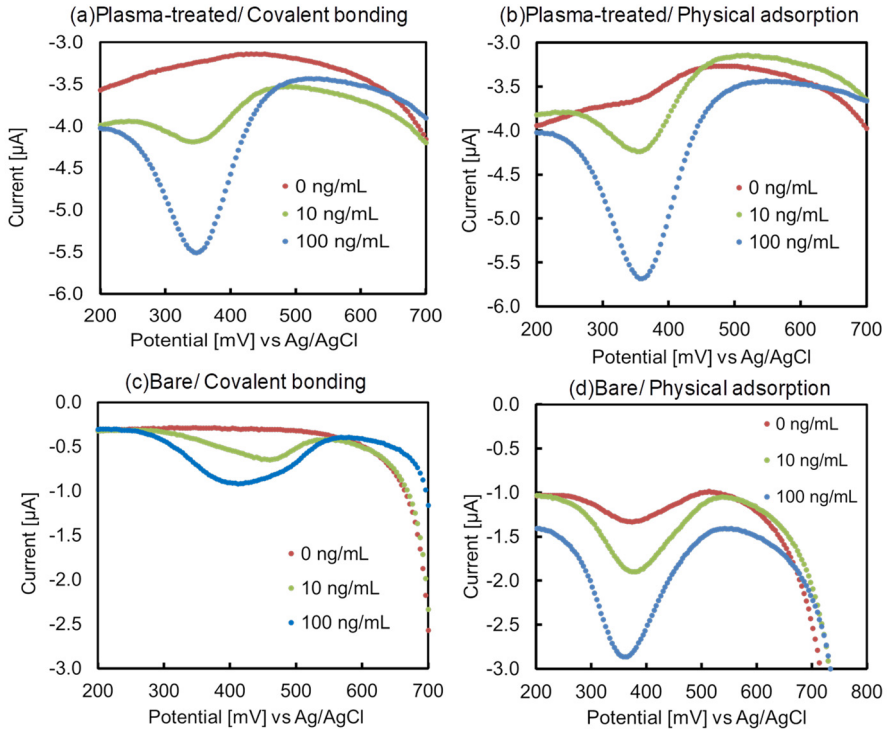

Figure 5. Differential pulse voltammograms of the pre-oxidized AuNPs immobilized on secondary antibody after sandwich immunoreaction in standard IgA solution (100, 10, 0 ng/mL) for plasma-treated/covalent bonding (**a**); plasma-treated electrode/physical adsorption (**b**); bare electrode/covalent bonding (**c**); and bare electrode/physical adsorption (**d**).

The voltammograms also showed an increase in the background current at the O_2-plasma-treated electrode. This may have been due to an increase in the charging current. In general, the charge current (i_{charge}) is given by Equation (2).

$$i_{charge} = \frac{E}{Rs} e^{-\frac{t}{RsC_{dl}}} \quad (2)$$

where E is applied potential, Rs is solution resistance, and t is potential applied time.

In other words, the increase in background current is associated with an increase in *Cdl*. In addition, the Faraday current could be detected even when the charge current was

increased. The results correlated with the relationship between the surface conditions and sensor sensitivity.

The calibration curves obtained from each voltammogram are shown in Figure 6a–d. The process of calculating LOD was examined more precisely because of its importance. LOD is generally defined as three times the variation (3σ) of the blank measurement which is divided by the slope of the linear response range. In the present case, LOD was calculated assuming a linear response at 0~50 ng/mL. In addition, a weighted slope was used to account for variations at each concentration. As a result, the weighted slopes are 0.039 (a), 0.029 (b), 0.014 (c) and 0.022 (d). Y intercepts (blank signal) were 0.010 ± 0.0064 (a), 0.38 ± 0.095 (b), 0.002 ± 0.0026 (c), 0.33 ± 0.0086 (d). The calculated LODs are also 0.50 ng/mL (a), 9.7 ng/mL (b), 0.56 ng/mL (c) and 1.2 ng/mL (d), as shown in Figure 6.

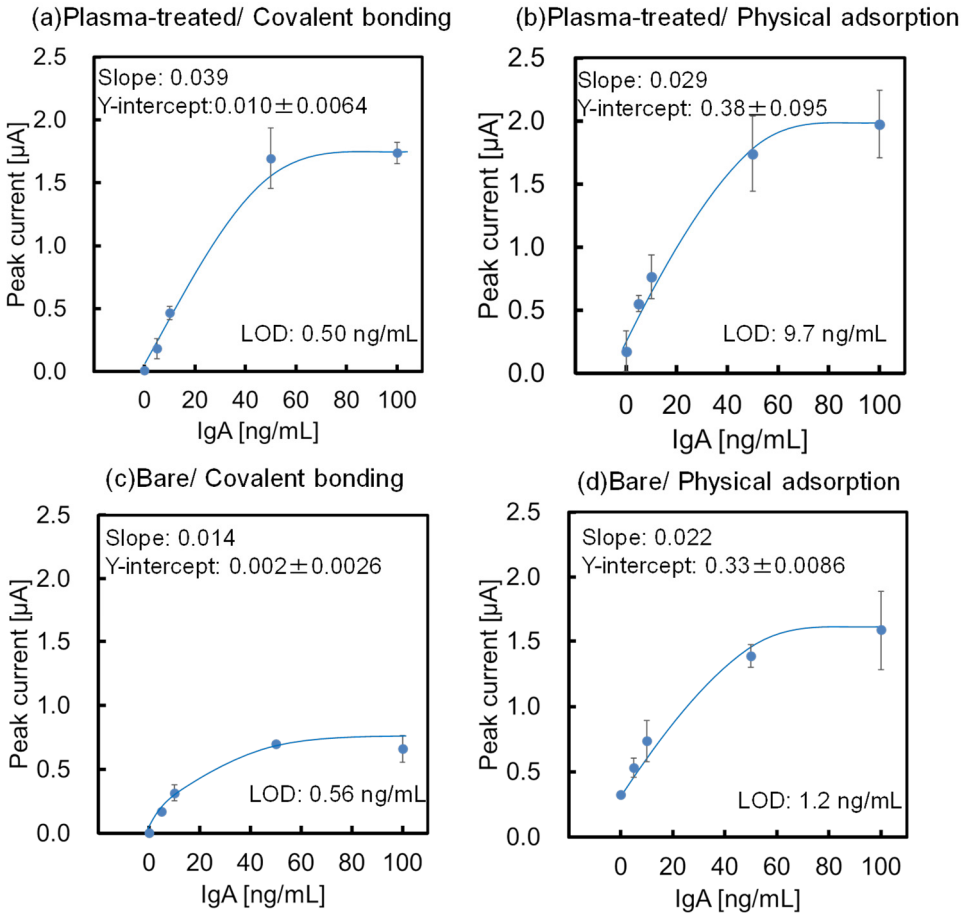

Figure 6. Calibration curves of IgA determination with the reduction peak intensity from pre-oxidized AuNP on plasma-treated electrode/covalent bonding (**a**); plasma-treated electrode/physical adsorption (**b**); bare electrode/covalent bonding (**c**); and bare electrode/physical adsorption (**d**).

Based on these results, we succeeded in increasing the sensitivity and LOD using an O_2-plasma-treated electrode and covalent-bonded antibody.

This is due to the improvement in the surface conditions of the electrode and the suppression of non-specific adsorption by covalent-bonded antibody. Table S1 lists the signal values, averages, and standard deviations of each calibration curve typically picked up in Figure 6a,d that were used in the LOD calculations. This also suggested that physical adsorption is possible at the O_2-plasma-treated electrodes (Figures 5b and 6b). It was inferred that antibody adsorption is based on unstable electrostatic interaction rather than hydrophobic interaction, which induced nonspecific adsorption as in the bare electrode. In this case, the variation of the blank signal is large.

Figure 6c shows a very effective LOD (0.56 ng/mL) but a very poor slope of 0.014. This is presumably due to the low amount of carboxyl groups present on the surface, which prevented the reaction of EDC/NHS, resulting in insufficient modification of the antibody. We have investigated the selectivity using the same antibodies and antigens as in the present study. We also investigated real saliva samples [62] and saliva reproduced samples [5] using a biosensor based on the same principle. The biosensor based on the AuNP showed sufficient selectivity. Therefore, the blank signals obtained in this study were attributed to the modification of the surface state by plasma treatment and EDC/NHS.

We observed the electrode surface immediately after reaction with 100 ng/mL of IgA using SEM and found the presence of AuNP on the electrode (Figure 7). We have performed elemental analysis of these particles using SEM-EDX in a previous study and have shown that they are Au [25]. The number of AuNPs were counted: 195 ± 47 for the O_2-plasma-treated electrode and 95 ± 24 for the bare electrode. This suggests that covalent bonding and O_2-plasma treatment can improve the amount and orientation of the antibodies. However, the linear response range is always constant, as can be seen in Figure 6, suggesting that the dissociation constant is also the same without the surface condition. Typically, comparing Figure 6a,d, there is no significant change in the current values obtained at 100 ng/mL of IgA. This may be due to the reduced reactivity with the negatively charged molecules, as shown in Figure 2, and therefore also with the negatively charged gold complexes ($[AuCl_4]^-$). This result correlates with Figure S2, which investigated the sensitivity to particle number by AuNPs directly on the plasma treatment electrode. The LOD of 190,000 particles on the O_2-plasma-treated electrode is well below the 6000 on the bare electrode that we previously reported [25].

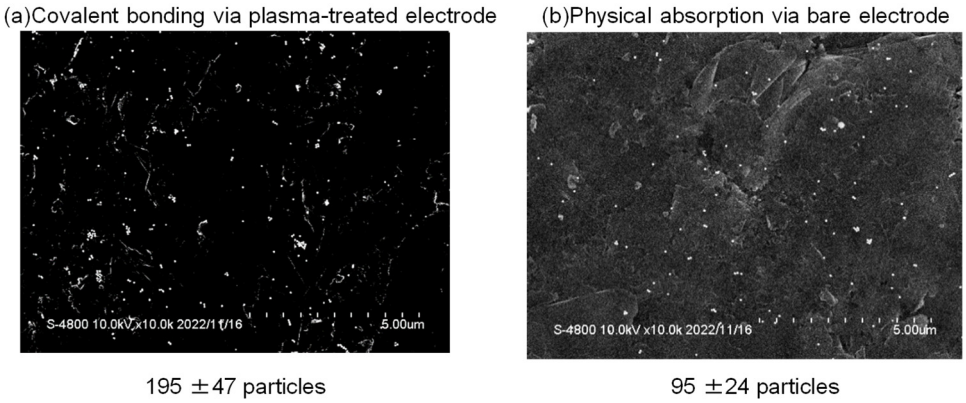

Figure 7. Scanning electron microscopy images observed from after antigen–antibody reaction on O_2-plasma-treated electrode and covalent bonding (**a**); and bare electrode and physical adsorption (**b**).

In general, the SEM showed the amount and orientation of antibody modification, and the EIS showed the electrochemical activity of the electrode, revealing the effects of O_2-plasma and covalent bonding on the antibody and electrode.

4. Conclusions

We investigated the modification of SPCE using O_2-plasma to develop highly sensitive electrochemical biosensors. XPS analysis and contact angle measurements of the O_2-plasma-treated electrode confirmed the generation of carboxyl groups and improved hydrophilicity. We also investigated the electrode surface using electrochemical methods such as CV and EIS. The results of both methods support the XPS and contact angle measurements, and the electrode surface was successfully modified. Therefore, we modified antibodies with common covalent bonding reagents, such as EDC/NHS, and four cases were compared: with and without O_2-plasma, and with and without covalent bonding.

The improvement rate with the O2-plasma and covalent bonding was 2.4 times higher with regard to the LOD and 1.8 times higher with regard to the slope compared to the

conventional method with the bare electrode and physical adsorption. The SEM images also suggested that antibody modification using covalent bonding on the plasma-treated electrode improved the amount of antibody modification. However, the electrochemical reactivity to the AuNPs was also reduced, limiting the improvement in sensitivity. As a result, we found a close relationship between the substituents, charge, and hydrophilicity of the electrode surface and electrochemical activity, which affects sensor sensitivity. Our findings relate to the relationship between the electrode surface conditions and sensor sensitivity and suggested that we might identify important factors in a discussion of antibody modification methods. There are a few simple and effective methods for surface modification of SPCE, including electrochemical activation, drop casting [65], and plasma treatment. By comparison, plasma treatment has the advantage of being able to treat many electrodes in a short time (5 s) and to generate carboxyl groups. It can also remove binders and dust from the electrode surface.

In the future, we plan to use the biosensors with improved sensitivity to measure previously undetectable biomarkers and develop the novel biosensors using the unique surface conditions generated by O_2-plasma.

Supplementary Materials: The following supporting information can be downloaded at: https://www.mdpi.com/article/10.3390/bios14040165/s1, Figure S1: Contact angle measurement of O_2-plasma-treated electrode. Table S1: Signal values used in the calibration curves. Figure S2: Differential pulse voltammograms (a) and Calibration curve (b) for AuNP modified on SPCE.

Author Contributions: Conceptualization, S.O. and E.T.; analysis, S.O., M.S. and E.T.; writing—original draft preparation, S.O.; writing—review and editing, M.S., H.N. and E.T.; supervision, E.T.; funding acquisition, S.O., H.N. and E.T. All authors have read and agreed to the published version of the manuscript.

Funding: This work was supported by JSPS KAKENHI (Grant Number JP15H05769) and operating expenses from AIST.

Institutional Review Board Statement: Not applicable.

Informed Consent Statement: Not applicable.

Data Availability Statement: The data that support the findings of this study are available from the corresponding authors upon reasonable request.

Conflicts of Interest: The authors declare no conflicts of interest.

References

1. Thiyagarajan, N.; Chang, J.-L.; Senthilkumar, K.; Zen, J.-M. Disposable electrochemical sensors: A mini review. *Electrochem. Commun.* **2014**, *38*, 86–90. [CrossRef]
2. Omidfar, K.; Dehdast, A.; Zarei, H.; Sourkohi, B.K.; Larijani, B. Development of urinary albumin immunosensor based on colloidal AuNP and PVA. *Biosens. Bioelectron.* **2011**, *26*, 4177–4183. [CrossRef] [PubMed]
3. Su, J.; Liu, W.; Chen, S.; Deng, W.; Dou, Y.; Zhao, Z.; Li, J.; Li, Z.; Yin, H.; Ding, X.; et al. A Carbon-Based DNA Framework Nano-Bio Interface for Biosensing with High Sensitivity and a High Signal-to-Noise Ratio. *ACS Sens.* **2020**, *5*, 3979–3987. [CrossRef] [PubMed]
4. Hartati, Y.W.; Komala, D.R.; Hendrati, D.; Gaffar, S.; Hardianto, A.; Sofiatin, Y.; Bahti, H.H. An aptasensor using ceria electrodeposited-screen-printed carbon electrode for detection of epithelial sodium channel protein as a hypertension biomarker. *R. Soc. Open Sci.* **2021**, *8*, 202040. [CrossRef] [PubMed]
5. Osaki, S.; Wakida, S.I.; Saito, M.; Tamiya, E. Towards On-site Determination of Secretory IgA in Artificial Saliva with Gold-Linked Electrochemical Immunoassay (GLEIA) Using Portable Potentiostat and Disposable Printed Electrode. *Appl. Biochem. Biotechnol.* **2021**, *193*, 1311–1320. [CrossRef] [PubMed]
6. de Araujo, W.R.; Lukas, H.; Torres, M.D.T.; Gao, W.; de la Fuente-Nunez, C. Low-Cost Biosensor Technologies for Rapid Detection of COVID-19 and Future Pandemics. *ACS Nano* **2024**, *18*, 1757–1777. [CrossRef] [PubMed]
7. Kumar, R.K.R.; Kumar, A.; Shaikh, M.O.; Liao, C.Y.; Chuang, C.H. Enzymeless electrochemical biosensor platform utilizing Cu_2O-Au nanohybrids for point-of-care creatinine testing in complex biological fluids. *Sens. Actuators B-Chem.* **2024**, *399*, 134787. [CrossRef]
8. Ganguly, A.; Lin, K.C.; Muthukumar, S.; Prasad, S. Autonomous, Real-Time Monitoring Electrochemical Aptasensor for Circadian Tracking of Cortisol Hormone in Sub-microliter Volumes of Passively Eluted Human Sweat. *ACS Sens.* **2021**, *6*, 63–72. [CrossRef]

9. Pusomjit, P.; Teengam, P.; Thepsuparungsikul, N.; Sanongkiet, S.; Chailapakul, O. Impedimetric determination of cortisol using screen-printed electrode with aptamer-modified magnetic beads. *Microchim. Acta* **2021**, *188*, 41. [CrossRef]
10. Tang, W.; Yin, L.; Sempionatto, J.R.; Moon, J.M.; Teymourian, H.; Wang, J. Touch-Based Stressless Cortisol Sensing. *Adv. Mater.* **2021**, *33*, e2008465. [CrossRef]
11. Gunasekaran, B.M.; Rajendran, G.K.; Rayappan, J.B.B.; Sivanesan, J.R.; Nesakumar, N.; Paulraj, A.W. Covalently Grafted 4-Aminopyridine-Reduced Graphene Oxide-Modified Screen-Printed Carbon Electrode for Electrochemical Sensing of Lead Ions. *Arab. J. Sci. Eng.* **2023**, *48*, 7721–7738. [CrossRef]
12. Hwang, J.H.; Fox, D.; Stanberry, J.; Anagnostopoulos, V.; Zhai, L.; Lee, W.H. Direct Mercury Detection in Landfill Leachate Using a Novel AuNP-Biopolymer Carbon Screen-Printed Electrode Sensor. *Micromachines* **2021**, *12*, 649. [CrossRef] [PubMed]
13. Biyani, M.; Biyani, R.; Tsuchihashi, T.; Takamura, Y.; Ushijima, H.; Tamiya, E.; Biyani, M. DEP-On-Go for Simultaneous Sensing of Multiple Heavy Metals Pollutants in Environmental Samples. *Sensors* **2016**, *17*, 45. [CrossRef] [PubMed]
14. Yamanaka, K.; Saito, M.; Kondoh, K.; Hossain, M.M.; Koketsu, R.; Sasaki, T.; Nagatani, N.; Ikuta, K.; Tamiya, E. Rapid detection for primary screening of influenza A virus: Microfluidic RT-PCR chip and electrochemical DNA sensor. *Analyst* **2011**, *136*, 2064–2068. [CrossRef] [PubMed]
15. Rasheed, P.A.; Sandhyarani, N. Electrochemical DNA sensors based on the use of gold nanoparticles: A review on recent developments. *Microchim. Acta* **2017**, *184*, 981–1000. [CrossRef]
16. Gupta, S.; Murthy, C.N.; Prabha, C.R. Recent advances in carbon nanotube based electrochemical biosensors. *Int. J. Biol. Macromol.* **2018**, *108*, 687–703. [CrossRef] [PubMed]
17. Yang, H. Highly Sensitive Electrochemical Biosensor Assembled by Au Nanoparticle /MOF-5 Composite Electrode for DNA Detection. *Int. J. Electrochem. Sci.* **2019**, *14*, 5491–5507. [CrossRef]
18. Khan, M.Z.H.; Hasan, M.R.; Hossain, S.I.; Ahommed, M.S.; Daizy, M. Ultrasensitive detection of pathogenic viruses with electrochemical biosensor: State of the art. *Biosens. Bioelectron.* **2020**, *166*, 112431. [CrossRef] [PubMed]
19. Feng, D.; Su, J.; Xu, Y.; He, G.; Wang, C.; Wang, X.; Pan, T.; Ding, X.; Mi, X. DNA tetrahedron-mediated immune-sandwich assay for rapid and sensitive detection of PSA through a microfluidic electrochemical detection system. *Microsyst. Nanoeng.* **2021**, *7*, 33. [CrossRef] [PubMed]
20. Ahmadi, A.; Shirazi, H.; Pourbagher, N.; Akbarzadeh, A.; Omidfar, K. An electrochemical immunosensor for digoxin using core-shell gold coated magnetic nanoparticles as labels. *Mol. Biol. Rep.* **2014**, *41*, 1659–1668. [CrossRef]
21. Duangkaew, P.; Tapaneeyakorn, S.; Apiwat, C.; Dharakul, T.; Laiwejpithaya, S.; Kanatharana, P.; Laocharoensuk, R. Ultrasensitive electrochemical immunosensor based on dual signal amplification process for p16(INK4a) cervical cancer detection in clinical samples. *Biosens. Bioelectron.* **2015**, *74*, 673–679. [CrossRef] [PubMed]
22. Yamanaka, K.; Vestergaard, M.C.; Tamiya, E. Printable Electrochemical Biosensors: A Focus on Screen-Printed Electrodes and Their Application. *Sensors* **2016**, *16*, 1761. [CrossRef] [PubMed]
23. Vasilescu, A.; Nunes, G.; Hayat, A.; Latif, U.; Marty, J.L. Electrochemical Affinity Biosensors Based on Disposable Screen-Printed Electrodes for Detection of Food Allergens. *Sensors* **2016**, *16*, 1863. [CrossRef]
24. Yang, M.H.; Choi, B.G.; Park, H.; Hong, W.H.; Lee, S.Y.; Park, T.J. Development of a Glucose Biosensor Using Advanced Electrode Modified by Nanohybrid Composing Chemically Modified Graphene and Ionic Liquid. *Electroanalysis* **2010**, *22*, 1223–1228. [CrossRef]
25. Osaki, S.; Espulgar, W.V.; Wakida, S.; Saito, M.; Tamiya, E. Optimization of electrochemical analysis for signal amplification in gold nanoparticle-probed immunoassays. *Electrochim. Acta* **2022**, *432*, 8. [CrossRef]
26. Nor, N.M.; Ramli, N.H.; Poobalan, H.; Tan, K.Q.; Razak, K.A. Recent Advancement in Disposable Electrode Modified with Nanomaterials for Electrochemical Heavy Metal Sensors. *Crit. Rev. Anal. Chem.* **2023**, *53*, 253–288. [CrossRef]
27. Shervedani, R.K.; Hatefi-Mehrjardi, A. Electrochemical characterization of directly immobilized glucose oxidase on gold mercaptosuccinic anhydride self-assembled monolayer. *Sens. Actuators B Chem.* **2007**, *126*, 415–423. [CrossRef]
28. Tricase, A.; Imbriano, A.; Macchia, E.; Picca, R.A.; Blasi, D.; Torsi, L.; Bollella, P. Electrochemical Investigation of Self-Assembling Monolayers toward Ultrasensitive Sensing. In Proceedings of the 2022 IEEE International Conference on Flexible and Printable Sensors and Systems (FLEPS), Vienna, Austria, 10–13 July 2022.
29. Wink, T.; vanZuilen, S.J.; Bult, A.; vanBennekom, W.P. Self-assembled monolayers for biosensors. *Analyst* **1997**, *122*, R43–R50. [CrossRef]
30. Campuzano, S.; Pedrero, M.; Montemayor, C.; Fatás, E.; Pingarrón, J.M. Characterization of alkanethiol-self-assembled monolayers-modified gold electrodes by electrochemical impedance spectroscopy. *J. Electroanal. Chem.* **2006**, *586*, 112–121. [CrossRef]
31. Ganesh, V.; Pal, S.K.; Kumar, S.; Lakshminarayanan, V. Self-assembled monolayers (SAMs) of alkoxycyanobiphenyl thiols on gold—A study of electron transfer reaction using cyclic voltammetry and electrochemical impedance spectroscopy. *J. Colloid Interface Sci.* **2006**, *296*, 195–203. [CrossRef]
32. Mandler, D.; Kraus-Ophir, S. Self-assembled monolayers (SAMs) for electrochemical sensing. *J. Solid State Electrochem.* **2011**, *15*, 1535–1558. [CrossRef]
33. Goda, T.; Miyahara, Y. Label-free and reagent-less protein biosensing using aptamer-modified extended-gate field-effect transistors. *Biosens. Bioelectron.* **2013**, *45*, 89–94. [CrossRef]

34. Zeng, Y.; Zhu, Z.-H.; Wang, R.-X.; Lu, G.-H. Electrochemical determination of bromide at a multiwall carbon nanotubes-chitosan modified electrode. *Electrochim. Acta* **2005**, *51*, 649–654. [CrossRef]
35. Wang, Q.; Zhang, B.; Lin, X.; Weng, W. Hybridization biosensor based on the covalent immobilization of probe DNA on chitosan–mutiwalled carbon nanotubes nanocomposite by using glutaraldehyde as an arm linker. *Sens. Actuators B Chem.* **2011**, *156*, 599–605. [CrossRef]
36. Lai, G.; Wang, L.; Wu, J.; Ju, H.; Yan, F. Electrochemical stripping analysis of nanogold label-induced silver deposition for ultrasensitive multiplexed detection of tumor markers. *Anal. Chim. Acta* **2012**, *721*, 1–6. [CrossRef] [PubMed]
37. Shirazi, H.; Ahmadi, A.; Darzianiazizi, M.; Kashanian, S.; Kashanian, S.; Omidfar, K. Signal amplification strategy using gold/N-trimethyl chitosan/iron oxide magnetic composite nanoparticles as a tracer tag for high-sensitive electrochemical detection. *IET Nanobiotechnol.* **2016**, *10*, 20–27. [CrossRef]
38. Kitikul, J.; Satienperakul, S.; Preechaworapun, A.; Pookmanee, P.; Tangkuaram, T. A Simple Flow Amperometric Electrochemical Biosensor Based on Chitosan Scaffolds and Gold Nanowires Modified on a Glassy Carbon Electrode for Detection of Glutamate in Food Products. *Electroanalysis* **2017**, *29*, 264–271. [CrossRef]
39. Muniandy, S.; Teh, S.J.; Thong, K.L.; Thiha, A.; Dinshaw, I.J.; Lai, C.W.; Ibrahim, F.; Leo, B.F. Carbon Nanomaterial-Based Electrochemical Biosensors for Foodborne Bacterial Detection. *Crit. Rev. Anal. Chem.* **2019**, *49*, 510–533. [CrossRef] [PubMed]
40. Viet, N.X.; Hoan, N.X.; Takamura, Y. Development of highly sensitive electrochemical immunosensor based on single-walled carbon nanotube modified screen-printed carbon electrode. *Mater. Chem. Phys.* **2019**, *227*, 123–129. [CrossRef]
41. Torres-Rivero, K.; Florido, A.; Bastos-Arrieta, J. Recent Trends in the Improvement of the Electrochemical Response of Screen-Printed Electrodes by Their Modification with Shaped Metal Nanoparticles. *Sensors* **2021**, *21*, 20. [CrossRef]
42. Wang, J.; Pedrero, M.; Sakslund, H.; Hammerich, O.; Pingarron, J. Electrochemical activation of screen-printed carbon strips. *Analyst* **1996**, *121*, 345–350. [CrossRef]
43. Sundaresan, P.; Chen, T.W.; Chen, S.M.; Tseng, T.W.; Liu, X.H. Electrochemical Activation of Screen Printed Carbon Electrode for the Determination of Antibiotic Drug Metronidazole. *Int. J. Electrochem. Sci.* **2018**, *13*, 1441–1451. [CrossRef]
44. Lu, Y.; Bao, C.Q.; Zou, J.; Xiao, J.L.; Zhong, W.; Gao, Y.S. Highly Sensitive Electrochemical Sensor for Sunset Yellow Based on Electrochemically Activated Glassy Carbon Electrode. *Molecules* **2022**, *27*, 5221. [CrossRef] [PubMed]
45. Erdem, A.; Senturk, H.; Yildiz, E.; Maral, M. Amperometric immunosensor developed for sensitive detection of SARS-CoV-2 spike S1 protein in combined with portable device. *Talanta* **2022**, *244*, 123422. [CrossRef] [PubMed]
46. Saito, M.; Kitsunai, M.; Ahmed, M.U.; Sugiyama, S.; Tamiya, E. Label-free electrochemical detection for food allergen using screen printed carbon electrode. *Electrochemistry* **2008**, *76*, 606–609. [CrossRef]
47. Kim, W.J.; Kim, S.; Lee, B.S.; Kim, A.; Ah, C.S.; Huh, C.; Sung, G.Y.; Yun, W.S. Enhanced protein immobilization efficiency on a TiO_2 surface modified with a hydroxyl functional group. *Langmuir* **2009**, *25*, 11692–11697. [CrossRef] [PubMed]
48. Daum, R.; Mrsic, I.; Hutterer, J.; Junginger, A.; Hinderer, S.; Meixner, A.J.; Gauglitz, G.; Chasse, T.; Schenke-Layland, K. Fibronectin adsorption on oxygen plasma-treated polyurethane surfaces modulates endothelial cell response. *J. Mater. Chem. B* **2021**, *9*, 1647–1660. [CrossRef] [PubMed]
49. Raj, J.; Herzog, G.; Manning, M.; Volcke, C.; MacCraith, B.D.; Ballantyne, S.; Thompson, M.; Arrigan, D.W. Surface immobilisation of antibody on cyclic olefin copolymer for sandwich immunoassay. *Biosens. Bioelectron.* **2009**, *24*, 2654–2658. [CrossRef]
50. Wasilewski, T.; Szulczynski, B.; Dobrzyniewski, D.; Jakubaszek, W.; Gebicki, J.; Kamysz, W. Development and Assessment of Regeneration Methods for Peptide-Based QCM Biosensors in VOCs Analysis Applications. *Biosensors* **2022**, *12*, 309. [CrossRef]
51. Tashima, D.; Hirano, M.; Kitazaki, S.; Eguchi, T.; Kumagai, S. Oxygen-Plasma Surface Treatment of an Electrode Sheet Using Carbon from Japanese Distilled Liquor Waste for Double-layer Capacitors. *Electrochem* **2020**, *1*, 323–327. [CrossRef]
52. Garcia, A.B.; Martinez-Alonso, A.; Leon y Leon, C.A.; Tascon, J.M.D. Modification of the surface properties of an activated carbon by oxygen plasma treatment. *Fuel* **1998**, *77*, 613–624. [CrossRef]
53. Sudhakara Prasad, K.; Muthuraman, G.; Zen, J.-M. The role of oxygen functionalities and edge plane sites on screen-printed carbon electrodes for simultaneous determination of dopamine, uric acid and ascorbic acid. *Electrochem. Commun.* **2008**, *10*, 559–563. [CrossRef]
54. Hojati-Talemi, P.; Zou, L.D.; Fabretto, M.; Short, R.D. Using oxygen plasma treatment to improve the performance of electrodes for capacitive water deionization. *Electrochim. Acta* **2013**, *106*, 494–499. [CrossRef]
55. Yuan, X.; Ma, L.; Zhang, J.; Zheng, Y. Simple pre-treatment by low-level oxygen plasma activates screen-printed carbon electrode: Potential for mass production. *Appl. Surf. Sci.* **2021**, *544*, 148760. [CrossRef]
56. Wang, J.; Xu, S.K.; Sun, P.C.; Du, H.Y.; Wang, L.D. Enhanced electrochemical performance of screen-printed carbon electrode by RF-plasma-assisted polypyrrole modification. *J. Mater. Sci.-Mater. Electron.* **2022**, *33*, 19923–19936. [CrossRef]
57. Ardhaoui, M.; Zheng, M.; Pulpytel, J.; Dowling, D.; Jolivalt, C.; Khonsari, F.A. Plasma functionalized carbon electrode for laccase-catalyzed oxygen reduction by direct electron transfer. *Bioelectrochemistry* **2013**, *91*, 52–61. [CrossRef] [PubMed]
58. Idegami, K.; Chikae, M.; Kerman, K.; Nagatani, N.; Yuhi, T.; Endo, T.; Tamiya, E. Gold Nanoparticle-Based Redox Signal Enhancement for Sensitive Detection of Human Chorionic Gonadotropin Hormone. *Electroanalysis* **2008**, *20*, 14–21. [CrossRef]
59. Xuan Viet, N.; Chikae, M.; Ukita, Y.; Maehashi, K.; Matsumoto, K.; Tamiya, E.; Hung Viet, P.; Takamura, Y. Gold-linked electrochemical immunoassay on single-walled carbon nanotube for highly sensitive detection of human chorionic gonadotropin hormone. *Biosens. Bioelectron.* **2013**, *42*, 592–597. [CrossRef]

60. Lim, S.A.; Yoshikawa, H.; Tamiya, E.; Yasin, H.M.; Ahmed, M.U. A highly sensitive gold nanoparticle bioprobe based electrochemical immunosensor using screen printed graphene biochip. *RSC Adv.* **2014**, *4*, 58460–58466. [CrossRef]
61. Gondoh-Noda, Y.; Kometani, M.; Nomura, A.; Aono, D.; Karashima, S.; Ushijima, H.; Tamiya, E.; Murayama, T.; Yoneda, T. Feasibility of a Novel Mobile C-Reactive Protein-Testing Device Using Gold-Linked Electrochemical Immunoassay: Clinical Performance Study. *JMIR Mhealth Uhealth* **2020**, *8*, e18782. [CrossRef]
62. Tamiya, E.; Osaki, S.; Tsuchihashi, T.; Ushijima, H.; Tsukinoki, K. Point-of-Care Diagnostic Biosensors to Monitor Anti-SARS-CoV-2 Neutralizing IgG/sIgA Antibodies and Antioxidant Activity in Saliva. *Biosensors* **2023**, *13*, 167. [CrossRef] [PubMed]
63. Jung, Y.; Kwak, J. Simultaneous Determination of Diffusion-Coefficient and Concentration by Chronoamperometry at a Microdisk Electrode. *Bull. Korean Chem. Soc.* **1994**, *15*, 209–213.
64. Kim, T.H.; Choi, H.S.; Go, B.R.; Kim, J. Modification of a glassy carbon surface with amine-terminated dendrimers and its application to electrocatalytic hydrazine oxidation. *Electrochem. Commun.* **2010**, *12*, 788–791. [CrossRef]
65. Wang, X.Y.; Zhang, Z.Q.; Wu, G.L.; Xu, C.X.; Wu, J.P.; Zhang, X.G.; Liu, J. Applications of electrochemical biosensors based on functional antibody-modified screen-printed electrodes: A review. *Anal. Methods* **2021**, *14*, 7–16. [CrossRef] [PubMed]